

One Step Closer: Creating the Future to Boost Monocular Semantic Scene Completion

Haoang Lu¹, Yuanqi Su^{1†}, Xiaoning Zhang¹ and Hao Hu²

Abstract—In recent years, visual 3D Semantic Scene Completion (SSC) has emerged as a critical perception task for autonomous driving due to its ability to infer complete 3D scene layouts and semantics from single 2D images. However, in real-world traffic scenarios, a significant portion of the scene remains occluded or outside the camera’s field of view - a fundamental challenge that existing monocular SSC methods fail to address adequately.

To overcome these limitations, we propose Creating the Future SSC (CF-SSC), a novel temporal SSC framework that leverages pseudo-future frame prediction to expand the model’s effective perceptual range. Our approach combines poses and depths to establish accurate 3D correspondences, enabling geometrically-consistent fusion of past, present, and predicted future frames in 3D space. Unlike conventional methods that rely on simple feature stacking, our 3D-aware architecture achieves more robust scene completion by explicitly modeling spatial-temporal relationships.

Comprehensive experiments on SemanticKITTI [1] and SSCBench-KITTI-360 [2], [3] benchmarks demonstrate state-of-the-art performance, validating the effectiveness of our approach, highlighting our method’s ability to improve occlusion reasoning and 3D scene completion accuracy.

I. INTRODUCTION

The rapid development of intelligent transportation systems demands robust environmental perception capabilities, particularly in complex urban scenarios where occlusions and limited sensor coverage pose significant challenges. As a fundamental task for autonomous driving and smart city infrastructure, 3D Semantic Scene Completion (SSC) bridges the critical gap between raw sensor inputs and comprehensive 3D environmental understanding. Traditional approaches relying on LiDAR [4]–[6] or multi-view systems [7]–[9] face inherent limitations in cost-effectiveness and deployment scalability, making monocular SSC an increasingly vital solution for next-generation transportation intelligence.

However, beyond its inherently ill-posed nature, monocular SSC faces additional practical constraints from the

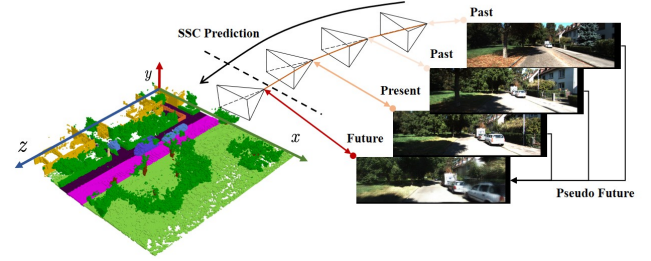


Fig. 1. The motivation of our approach: Predicting pseudo future frames from past frames to achieve “seeing ahead” and monocular SSC.

limited field-of-view (FoV) of single cameras. This severe visibility constraint fundamentally limits the reliability of conventional monocular SSC systems [10]–[12], which process each frame in isolation. While introducing temporal information from past frames could theoretically expand the observable range, in practice these frames (captured from positions behind the current viewpoint) provides limited benefits for forward occlusions in the driving direction. To truly extend the perceptual range of monocular SSC we need to “get one step closer” by leveraging future frames.

Therefore, in this paper, we propose a novel framework that utilizes pseudo-future frame prediction to effectively “see ahead” in the scene. Following previous monocular SSC methods [12]–[14], we utilize a pre-trained depth prediction model to estimate depth maps for past and current frames. Based on the predicted depth maps and relative poses, we derive optical flow and use it to generate preliminary future frame images and depth maps, which are further refined using a FutureSynthNet to obtain high-quality pseudo-images and pseudo-depth maps of future frames. Finally, by integrating the predicted depth maps and poses, we consolidate all frame information into a unified 3D space for Semantic Scene Completion (SSC).

In contrast to previous temporal monocular SSC methods [13]–[15] that naively concatenate multi-frame inputs and consequently suffer from geometric ambiguity, our approach achieves temporally coherent 3D fusion through integration of sequential context. Furthermore, by incorporating future frame prediction, we significantly extend the visible scope of SSC, enabling the system to truly “see ahead” and anticipate occluded or emerging structures, shown in Fig.1.

Based on the aforementioned modules and methodologies, we present Creating the Future SSC (CF-SSC), an

[†]Corresponding Author. Email: yuanqisu@mail.xjtu.edu.cn

The research was supported by the Science and Technology Research and Development Plan of China State Railway Group Co., Ltd. (No. RITS2023KF03) and the National Natural Science Foundation of China (No. 62473306, No. U24B20181).

¹Haoang Lu, Yuanqi Su and Xiaoning Zhang are with School of Computer Science and Technology, Xi’an Jiaotong University, Xi’an, Shaanxi, China. Orcid: 0009-0008-4514-1110, 0000-0001-7520-7020, 0000-0002-0583-4616

²Hao Hu is with The Institute of Computing, China Academy of Railway Sciences Corporation and The Center of National Railway Intelligent Transportation System Engineering and Technology. Orcid: 0000-0002-9422-750X

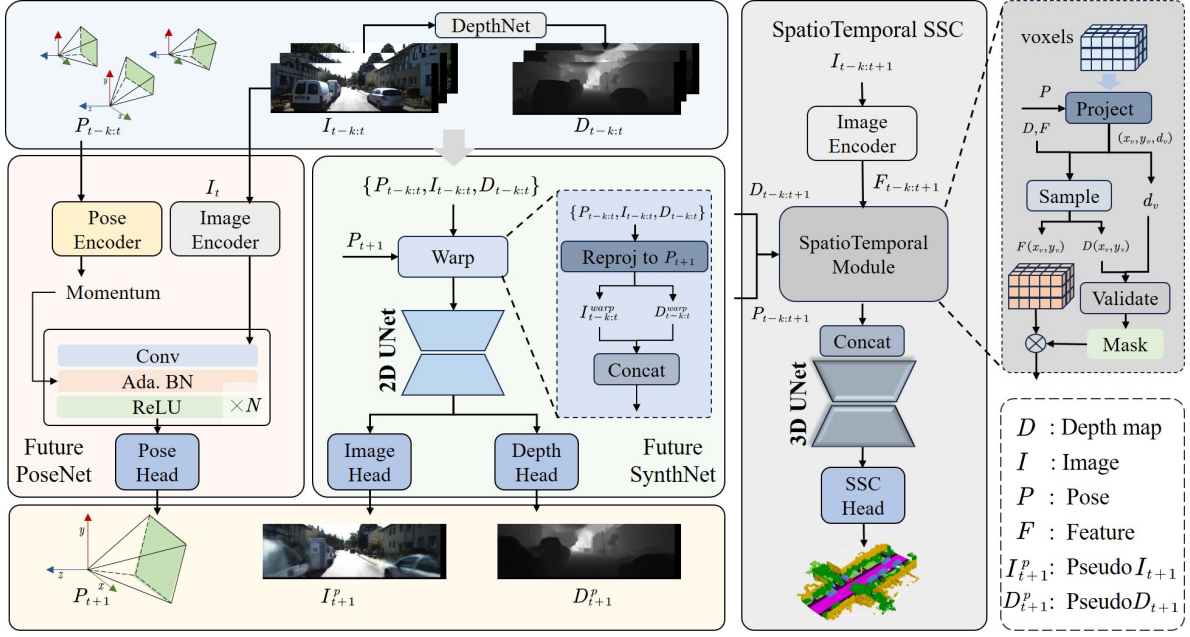


Fig. 2. Overall framework of our proposed CF-SSC, which takes images and poses of past frames and the current frame as input, predicts images, depth, and relative poses of future frames, and integrates all temporal information for SSC.

innovative monocular SSC framework that effectively combines 3D geometric reconstruction with future frame prediction. We have conducted extensive experiments on two established benchmark datasets, SemanticKITTI [1] and SSCBench-KITTI-360 [2], [3], to thoroughly validate our approach, which achieves state-of-the-art performance. The key contributions of our work are summarized as follows:

- We propose a novel pseudo-future based monocular SSC framework that effectively extends the visible range of monocular SSC through future frame image and depth map prediction. This innovative approach achieves the “see ahead” capability, successfully addressing the limited visible range problem inherent in conventional monocular SSC methods.
- By combining relative poses with depth prediction, we develop a geometrically consistent temporal monocular SSC method. This 3D-aware fusion effectively eliminates the geometric ambiguity present in previous temporal approaches [13]–[15].
- We conducted extensive experiments on both SemanticKITTI [4] and SSCBench-KITTI-360 [2], [3] datasets to validate our TempSSC framework. The results demonstrate its effectiveness and show state-of-the-art performance.

II. RELATED WORK

A. Semantic Scene Completion

3D Semantic Scene Completion (SSC) aims to reconstruct a voxelized 3D scene by predicting both occupancy (geometric completeness) and semantic labels for all voxels within a predefined volume. This task was first formally introduced by [4], establishing a unified framework for

joint geometric and semantic inference. Due to its ability to provide dense 3D scene layouts—critical for path planning and obstacle avoidance—SSC has emerged as a pivotal perception task in autonomous driving and robotics.

Early SSC methods [5], [6], [16], [17] predominantly relied on dense depth input (e.g., LiDAR point clouds or depth maps) to achieve high-fidelity 3D reconstruction. While demonstrating impressive results, their dependence on expensive sensors significantly limited practical deployment scalability.

Recent years have witnessed the rise of vision-based SSC approaches, attracting growing research interest. Notably, [18] proposed a versatile framework applicable to various 3D vision tasks, while [9] introduced an efficient tri-plane 3D feature representation that reduces memory requirements. For temporal information fusion, [19] developed a novel cost volume approach, and [8] proposed Hierarchical Temporal Context Learning. Although these stereo/multi-camera based methods offer lower deployment costs than LiDAR-dependent solutions, they still face inherent limitations including multi-camera system calibration challenges and incompatibility with monocular image inputs.

B. Monocular Semantic Scene Completion

The field witnessed a significant advancement when [10] first proposed a purely vision-based monocular SSC solution, which sampled image features by projecting voxel positions onto 2D planes. This work was subsequently improved by [11] through the introduction of Normalized Device Coordinates (NDC) to optimize the 2D-to-3D lifting scheme.

A crucial development came with [13], who pioneered

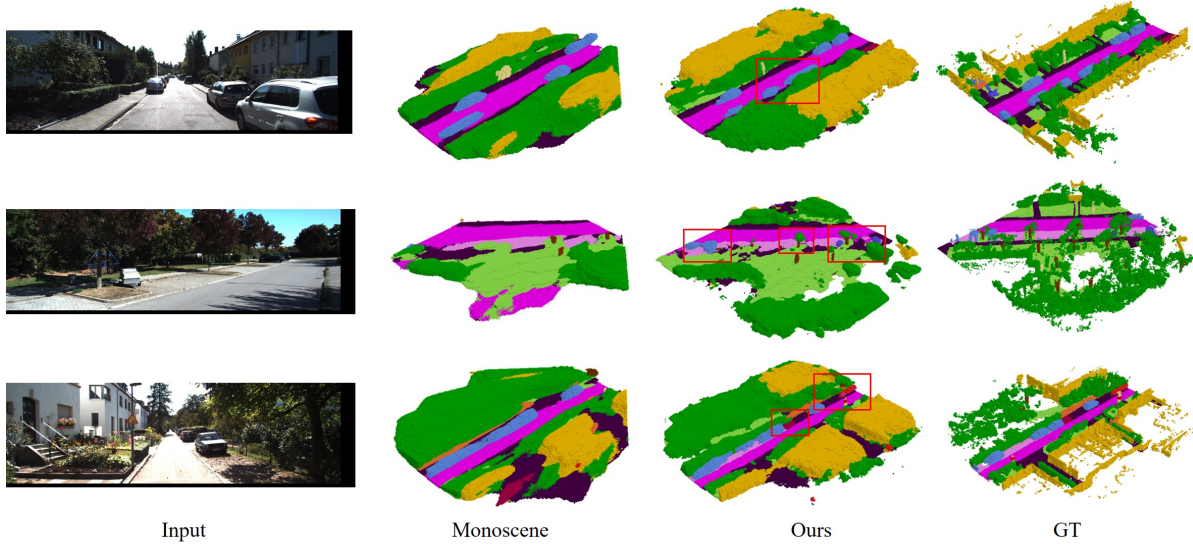


Fig. 3. Visualization results of our method on the SemanticKITTI [1] dataset along with comparisons against MonoScene [10].

the integration of depth prediction with monocular SSC. Their approach utilized a pre-trained depth predictor to generate depth maps, enabling active projection of image features into 3D space. This design paradigm has been consistently maintained in subsequent works [12], [14], [15], [20] (including our depth predictor implementation), with some studies introducing incremental improvements to this framework.

Despite progress in monocular SSC, the limited field of view remains a core challenge. We address this by leveraging future frame prediction to extend perception beyond the current observation.

C. Future Frame Prediction

Future frame prediction aims to forecast upcoming frames based on past frame information. Depending on the prediction objectives, it can generally be categorized into optical flow-based methods [21], [22] and direct image generation methods [23], [24]. These approaches can be further divided into deterministic synthesis [25], [26] and stochastic synthesis [27], [28] based on their generation mechanisms.

As our goal is accurate future frame prediction rather than realism, we adopt deterministic synthesis. Focusing on occluded regions, which challenge optical flow assumptions, we use direct image generation. To meet real-time demands in traffic scenarios, we also avoid diffusion-based models [29]–[31].

III. METHOD

A. Overview

As shown in Fig.2, our method first feeds the relative pose sequence of past frames $P_{t-k:t}$ and the current frame I_t into the FuturePoseNet to predict future frame poses P_{t+1}^p . Next, we compute the optical flow between future frames and both current and past frames using the predicted depth maps and

relative poses, generating initial pseudo-future frames and their corresponding depth. These are then refined by the FutureSynthNet to produce the final predicted future frames and depth maps.

Finally, all frames, along with their depth maps and poses, are fed into the SpatioTemporal SSC, where image features are projected into a unified 3D space for geometrically consistent temporal integration.

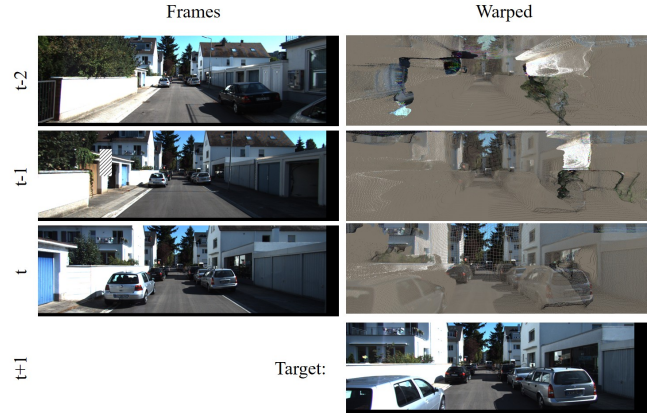


Fig. 4. Visualization of warping past and current frames to future frame.

B. FuturePoseNet

To predict the direction of the next frame's pose, we need two pieces of information: the current vehicle's momentum and the current road information, which we obtain from the pose sequence of past frames $P_{t-k:t}$ and the current frame's image I_t , respectively. As shown in Fig.2, we first use the current frame's image feature into 3D, using the same method as in SpatioTemporal SSC (but using only a single frame) and obtain the 3D feature. Next, we encode the pose sequence of past frames $P_{t-k:t}$ to derive

TABLE I
QUANTITATIVE RESULTS ON THE HIDDEN TEST SET OF SEMANTICKITTI [1], WHERE THE HIGHEST AND SECOND-HIGHEST SCORES FOR EACH METRIC ARE HIGHLIGHTED IN **BOLD** AND UNDERLINE, RESPECTIVELY.

Method	Date	IoU \uparrow	mIoU \uparrow	road	sidewalk	parking	other-grnd.	building	car	truck	bicycle	motorcycle	other-veh.	vegetation	trunk	terrain	person	bicyclist	motorcyclist	fence	pole	traf.-sign
Stereo camera-based methods																						
StereoScene [7]	IJCAI2024	43.34	15.36	61.90	31.20	30.70	10.70	24.20	22.80	2.80	3.40	2.40	6.10	23.80	8.40	27.00	2.90	2.20	0.50	16.50	7.00	7.20
HTCL-S [8]	ECCV2024	44.23	17.09	64.40	34.80	33.80	12.40	25.90	27.30	5.70	1.80	2.20	5.40	25.30	10.80	31.20	1.10	3.10	0.90	21.10	9.00	8.30
Monocular camera-based methods																						
MonoScene [10]	CVPR2023	34.16	11.08	54.70	27.10	24.80	5.70	14.40	18.80	3.30	0.50	0.70	4.40	14.90	2.40	19.50	1.00	1.40	0.40	11.10	3.30	2.10
TPVFormer [9]	CVPR2023	34.25	11.26	55.10	27.20	27.40	6.50	14.80	19.20	3.70	1.00	0.50	2.30	13.90	2.60	20.40	1.10	2.40	0.30	11.00	2.90	1.50
SurroundOcc [32]	ICCV2023	34.72	11.86	56.90	28.30	30.20	6.80	15.20	20.60	1.40	1.60	1.20	4.40	14.90	3.40	19.30	1.40	2.00	0.10	11.30	3.90	2.40
OccFormer [33]	ICCV2023	34.53	12.32	55.90	30.30	31.50	6.50	15.70	21.60	1.20	1.50	1.70	3.20	16.80	3.90	21.30	2.20	1.10	0.20	11.90	3.80	3.70
IAMSSC [34]	T-ITS2024	43.74	12.37	54.00	25.50	24.70	6.90	19.20	21.30	3.80	1.10	0.60	3.90	22.70	5.80	19.40	1.50	2.90	0.50	11.90	5.30	4.10
VoxFormer-T [13]	CVPR2023	43.21	13.41	54.10	26.90	25.10	7.30	23.50	21.70	3.60	1.90	1.60	4.10	24.40	8.10	24.20	1.60	1.10	0.00	13.10	6.60	5.70
DepthSSC [35]	arXiv2024	44.58	13.11	55.64	27.25	25.72	5.78	20.46	21.94	3.74	1.35	0.98	4.17	23.37	7.64	21.56	1.34	2.79	0.28	12.94	5.87	6.23
Symphonize [12]	CVPR2024	42.19	15.04	58.40	29.30	26.90	<u>11.70</u>	<u>24.70</u>	23.60	3.20	<u>3.60</u>	<u>2.60</u>	5.60	24.20	10.00	23.10	3.20	1.90	2.00	16.10	7.70	8.00
HASSC-T [20]	CVPR2024	42.87	14.38	55.30	29.60	25.90	11.30	23.10	23.00	2.90	1.90	1.50	4.90	24.80	9.80	<u>26.50</u>	1.40	<u>3.00</u>	0.00	14.30	7.00	7.10
H2GFormer-T [14]	AAAI2024	43.52	14.60	57.90	30.40	30.00	6.90	24.00	23.70	<u>5.20</u>	0.60	1.20	5.00	<u>25.20</u>	<u>10.70</u>	25.80	1.10	0.10	0.00	14.60	<u>7.50</u>	9.30
MonoOcc-L [15]	ICRA2024	-	<u>15.63</u>	<u>59.10</u>	<u>30.90</u>	27.10	9.80	22.90	<u>23.90</u>	7.20	4.50	2.40	7.70	25.00	9.80	26.10	<u>2.80</u>	4.70	<u>0.60</u>	<u>16.90</u>	7.30	8.40
CF-SSC-Online	-	46.21	16.40	61.30	33.30	<u>29.20</u>	11.90	30.40	26.30	4.80	2.60	2.70	<u>6.30</u>	28.50	11.40	28.30	1.50	1.40	0.40	17.70	7.20	6.30
CF-SSC-Offline	-	48.25	17.70	62.20	34.80	30.70	12.90	31.70	27.70	6.00	3.50	3.50	6.20	31.60	12.90	29.90	2.20	2.80	0.80	19.10	9.10	8.70

the vehicle’s momentum feature M_t . Finally, we employ a 3D U-Net network, replacing all batch normalization [36] layers with adaptive batch normalization [37], and use the vehicle’s momentum feature M_t to modulate the 3D feature, ultimately predicting the next frame’s pose P_{t+1}^p .

This approach integrates vehicle dynamics with 3D scene understanding for robust future pose prediction, using adaptive 3D feature modulation to ensure accurate motion forecasting and geometric consistency.

C. FutureSynthNet

By leveraging predicted depth maps of current and past frames $D_{t-k:t}$, along with relative poses between past-current frames and future-current frames (predicted by FuturePoseNet) $P_{t-k:t+1}$, we reproject past and current images onto the future frame. This allows us to generate pseudo-future frames and corresponding depth maps through warping. As shown in the Fig.4, the generation quality degrades for frames temporally distant from the target future frame due to object motion.

These pseudo-future results are then refined by FutureSynthNet (a U-Net based network) to produce optimized predictions. Notably, during FutureSynthNet training, we preserve 3D consistency by employing both L1 loss against ground truth and a feature-level loss computed using SpatioTemporal SSC’s backbone network.

D. SpatioTemporal SSC

As shown in Fig.2, SpatioTemporal SSC consists of three components: a 2D backbone, a spatiotemporal module, and a 3D U-Net. The 2D backbone extracts 2D features

from each frame’s image, while the spatiotemporal module spatially aligns information across all temporal frames and sample from the 2D features to form a unified 3D feature volume. Finally, this 3D feature volume is fed into the 3D U-Net for further feature extraction and SSC prediction.

In the spatiotemporal module, to spatially align information across all temporal frames, we project all voxels within the current frame’s scene range S onto each frame’s image plane using the relative poses between past/future frames and the current frame, obtaining projection coordinates (x_v, y_v, d_v) . The visibility of each voxel is then determined by comparing its projected depth d_v with the predicted depth value at the corresponding location in the target frame’s depth map $D(x_v, y_v)$ as:

$$V := \{v | v \in S, |d_v - D(x_v, y_v)| \leq \theta_d\} \quad (1)$$

where θ_d is set to 0.5 meters in experiments to compensate for errors in depth estimation.

To reduce computational cost, we downsample the voxel grid by grouping $4 \times 4 \times 4$ voxels into blocks. A block is marked visible if any voxel within it is visible, with projection coordinates averaged over visible voxels. For each visible block, 2D features are sampled from corresponding frames and concatenated (zero-padded if absent) to form the final 3D feature, which is input into the 3D U-Net for SSC.

E. Losses

In the CF-SSC framework, since training FutureSynthNet requires supervision in SpatioTemporal SSC’s feature space, we decouple the training of SpatioTemporal SSC from other modules. For SpatioTemporal SSC specifically, following

TABLE II

QUANTITATIVE RESULTS ON THE TEST SET OF SSCBENCH-KITTI-360 [2], [3], WHERE THE HIGHEST AND SECOND-HIGHEST SCORES FOR EACH METRIC ARE HIGHLIGHTED IN **BOLD** AND UNDERLINE, RESPECTIVELY.

Method	Date	IoU↑	mIoU↑	car	bicycle	motorcycle	truck	other-veh.	person	road	parking	sidewalk	other-grnd.	building	fence	vegetation	terrain	pole	traf.-sign	other-struct.	other-obj.
LiDAR-based methods																					
SSCNet [4]	CVPR2017	53.58	16.95	31.95	0.00	0.17	10.29	0.00	0.07	65.70	17.33	41.24	3.22	44.41	6.77	43.72	28.87	0.78	0.75	8.69	0.67
LMSCNet [5]	3DV 2020	47.35	13.65	20.91	0.00	0.00	0.26	0.58	0.00	62.95	13.51	33.51	0.20	43.67	0.33	40.01	26.80	0.00	0.00	3.63	0.00
Monocular camera-based methods																					
MonoScene [10]	CVPR2023	37.87	12.31	19.34	0.43	0.58	8.02	2.03	0.86	48.35	11.38	28.13	3.32	32.89	3.53	26.15	16.75	6.92	5.67	4.20	3.09
TPVFormer [9]	CVPR2023	40.22	13.64	21.56	1.09	1.37	8.06	2.57	2.38	52.99	11.99	31.07	3.78	34.83	4.80	30.08	17.52	7.46	5.86	5.48	2.70
OccFormer [33]	ICCV2023	40.27	13.81	22.58	0.66	0.26	9.89	3.82	2.77	54.30	13.44	31.53	3.55	36.42	4.80	31.00	19.51	7.77	8.51	6.95	4.60
VoxFormer [13]	CVPR2023	38.76	11.91	17.84	1.16	0.89	4.56	2.06	1.63	47.01	9.67	27.21	2.89	31.38	4.97	28.99	14.69	6.51	6.92	3.79	2.43
IAMSSC [34]	T-ITS2024	41.80	12.97	18.53	<u>2.45</u>	1.76	5.12	3.92	3.09	47.55	10.56	28.35	4.12	31.53	6.28	29.17	15.24	8.29	7.01	6.35	4.19
DepthSSC [35]	arXiv2024	40.85	14.28	21.90	2.36	4.30	11.51	4.56	2.92	50.88	12.89	30.27	2.49	37.33	5.22	29.61	21.59	5.97	7.71	5.24	3.51
Symphonies [12]	CVPR2024	<u>44.12</u>	<u>18.58</u>	30.02	1.85	<u>5.90</u>	25.07	12.06	8.20	<u>54.94</u>	<u>13.83</u>	<u>32.76</u>	6.93	35.11	8.58	38.33	11.52	<u>14.01</u>	<u>9.57</u>	14.44	11.28
CF-SSC-Online	-	45.79	19.10	<u>28.10</u>	3.39	6.87	<u>16.76</u>	<u>7.75</u>	<u>5.68</u>	59.01	16.80	37.60	<u>4.95</u>	42.16	<u>8.26</u>	<u>36.14</u>	21.89	14.73	17.72	<u>9.73</u>	<u>7.14</u>
CF-SSC-Offline	-	47.38	19.83	28.51	3.70	6.91	17.38	7.96	6.61	62.04	17.99	39.83	4.99	42.44	8.66	38.26	24.67	15.06	18.35	9.76	7.87

[10], we employ Scene-Class Affinity Loss L_{scal} with dual supervision on both geometric and semantic aspects, combined with cross-entropy loss weighted by class frequencies. The complete loss function is formulated as:

$$L = L_{scal}^{geo} + L_{scal}^{sem} + L_{ce} \quad (2)$$

For FuturePoseNet, following [38], we supervise it using MSE loss. For the future frame images predicted by FutureSynthNet, we apply L1 loss supervision in both image space and feature space, along with SSIM loss for geometric constraints, while using L1 loss to supervise its predicted depth map. The complete loss function is formulated as:

$$L = L_{mse}^p + L_{l1}^{img} + L_{l1}^{feat} + L_{ssim}^{img} + L_{l1}^d \quad (3)$$

The weight for the L_{mse}^p loss is set to 0.1, and the weights for all other losses are set to 1.

IV. EXPERIMENTS

A. Datasets and Evaluation Metrics

We conduct experiments on two widely-used real-world traffic scene SSC datasets, SemanticKITTI [1] and SSCBench-KITTI-360 [2], [3]. Both datasets set the scene range to $51.2\text{m} \times 51.2\text{m} \times 6.4\text{m}$ and define each voxel as a cube with 0.2m edge length, resulting in a $256 \times 256 \times 32$ scene resolution. The SemanticKITTI dataset contains 10 training sequences (3,834 samples), 1 validation sequence (815 samples), and 11 hidden test sequences (3,992 samples), with 20 valid classes and 1 invalid class. The SSCBench-KITTI-360 dataset contains 7 training sequences (8,487 samples), 1 validation sequence (1,812 samples), and 1 test sequence (2,566 samples), with 19 valid classes. Consistent with prior SSC tasks,

Consistent with prior SSC tasks, we employ Intersection over Union (IoU) and mean IoU (mIoU) as evaluation

metrics. The IoU metric primarily assesses the model’s capability in reconstructing scene geometry, while mIoU evaluates its performance in recovering semantic information of the scene.

TABLE III

ABLATION STUDY ON TEMPORAL INTEGRATION METHODS.

Methods	IoU↑	mIoU↑
Concatenation	44.5	14.7
Spatiotemporal Module	48.6 (+4.1)	17.0 (+2.3)

TABLE IV

ABLATION STUDY FOR TEMPORAL INPUT ON SPATIOTEMPORAL SSC.

t	-20	-15	-10	-5	0	+5	+5p	IoU↑	mIoU↑
Offline	✓	✓	✓	✓	✓	✓		46.2	15.7
					✓	✓		48.6	17.0
					✓			43.7	14.3
Online	✓	✓	✓	✓	✓			45.8	14.8
					✓			46.3	14.9
					✓		✓	46.8	16.0
					✓		✓	44.3	15.2

B. Implementation Details

We train our model using 4 NVIDIA RTX 4090 GPUs. Following previous methods [10], we set the batch size to 4 and employ the AdamW [39] optimizer for 30 epochs. The initial learning rate is set to $1\text{e-}4$ with weight decay of $1\text{e-}4$, and the learning rate is reduced by a factor of 0.1 at the 20th and 25th epochs.

Both SpatioTemporal SSC and FuturePoseNet use ResNet-50 [40] as the backbone, initialized with



Fig. 5. Visualization of occlusion handling.

MaskDINO-pretrained weights [41], following [12]. The 3D U-Net, based on [5], [10], applies two downsampling and upsampling stages, with each $3 \times 3 \times 3$ convolution decomposed into three $3 \times 1 \times 1$ convolutions to reduce parameters. For depth estimation, we adopt the off-the-shelf method from [13], a standard choice in prior works [12], [14], [15], [20], [35].

Additionally, as mentioned earlier, we use a frame interval of 5 frames between consecutive inputs

C. Main Results

We conducted comparisons with a series of state-of-the-art (SOTA) methods on the SemanticKITTI [1] and SSCBench-KITTI-360 [2], [3] datasets, as shown in Tab.I and Tab.II. Here, **offline** methods utilize ground-truth future frame information and can only operate in offline mode. These are included in the table for reference but are not directly compared with other methods. In contrast, **online** methods rely solely on the current and past frames and are compared against other approaches.

As shown in the results, our CF-SSC (online version) achieves 16.4% mIoU on the SemanticKITTI dataset, surpassing all existing monocular SSC methods. Notably, our approach even outperforms StereoScene [7], a novel stereo SSC method. On the SSCBench-KITTI-360 dataset, we also achieve 19.1% mIoU, exceeding the current SOTA methods. These results demonstrate that “seeing ahead” significantly enhances monocular SSC performance.

Finally, We provide a visual comparison between our SSC predictions and MonoScene [10] on the SemanticKITTI dataset, as illustrated in the Fig.3. Our method demonstrates superior object recognition and scene reconstruction.

As shown in the Fig.5, we use L1 loss on primary features to suppress artifacts, resulting in blurry outputs. While mildly occluded regions are reconstructed well, severe occlusions remain challenging.

D. Ablations

We conduct comprehensive ablation studies on the SemanticKITTI [1] validation set to evaluate: (1) the impact of different temporal integration methods on network performance, (2) the effect of temporal frame inputs on

SpatioTemporal SSC, and the performance gains from incorporating pseudo future frames, pseudo depth maps, and predicted future frame poses.

The Role of SpatialTemporal Module. As shown in Tab.III, we compare different temporal integration methods for SSC, where both models take 4 past frames and 1 future frame as additional inputs with a 5-frame interval. The baseline “concatenation” method (commonly adopted in previous works) directly concatenates 2D features from different frames with the current frame’s 2D features before lifting them to 3D space using the current frame’s predicted depth for SSC. Our SpatioTemporal Module significantly improves both IoU and mIoU metrics, demonstrating its effectiveness and highlighting the benefits of temporal feature integration in 3D space rather than 2D space.

Different Temporal Input. We conduct a comprehensive analysis of different temporal input configurations’ impact on model performance (as shown in Tab.IV), where +5p represents using our predicted pseudo future frames, depth maps, and poses. Optimal results require ground-truth future frames, which are unavailable online. In practical settings, current-frame-only input performs worst; adding past frames yields limited gains due to viewpoint misalignment. Our framework significantly improves performance by integrating FutureSynthNet-generated pseudo future frames and depth maps with FuturePoseNet-predicted poses.

V. CONCLUSION

In this paper, we present CF-SSC, a temporal SSC framework that tackles monocular SSC’s limited observation range by predicting future frames from past observations. Experiments show SOTA performance on SemanticKITTI and SSCBench-KITTI-360. We hope this work inspires future research in temporal 3D scene understanding, advancing monocular perception in dynamic environments.

REFERENCES

- [1] J. Behley, M. Garbade, A. Milioto, J. Quenzel, S. Behnke, C. Stachniss, and J. Gall, “Semantickitti: A dataset for semantic scene understanding of lidar sequences,” in *Proceedings of the IEEE/CVF international conference on computer vision*, 2019, pp. 9297–9307.

- [2] Y. Li, S. Li, X. Liu, M. Gong, K. Li, N. Chen, Z. Wang, Z. Li, T. Jiang, F. Yu, Y. Wang, H. Zhao, Z. Yu, and C. Feng, "Sscbench: A large-scale 3d semantic scene completion benchmark for autonomous driving," in *2024 IEEE/RSJ International Conference on Intelligent Robots and Systems (IROS)*, 2024.
- [3] Y. Liao, J. Xie, and A. Geiger, "Kitti-360: A novel dataset and benchmarks for urban scene understanding in 2d and 3d," *IEEE Transactions on Analysis and Machine Intelligence*, vol. 45, no. 3, pp. 3292–3310, 2022.
- [4] S. Song, F. Yu, A. Zeng, A. X. Chang, M. Savva, and T. Funkhouser, "Semantic scene completion from a single depth image," in *Proceedings of the IEEE conference on computer vision and pattern recognition*, 2017, pp. 1746–1754.
- [5] L. Roldao, R. De Charette, and A. Verroust-Blondet, "Lmscnet: Lightweight multiscale 3d semantic completion," in *2020 International Conference on 3D Vision (3DV)*. IEEE, 2020, pp. 111–119.
- [6] X. Yan, J. Gao, J. Li, R. Zhang, Z. Li, R. Huang, and S. Cui, "Sparse single sweep lidar point cloud segmentation via learning contextual shape priors from scene completion," in *Proceedings of the AAAI conference on artificial intelligence*, vol. 35, no. 4, 2021, pp. 3101–3109.
- [7] B. Li, Y. Sun, Z. Liang, D. Du, Z. Zhang, X. Wang, Y. Wang, X. Jin, and W. Zeng, "Bridging stereo geometry and bev representation with reliable mutual interaction for semantic scene completion," *arXiv preprint arXiv:2303.13959*, 2023.
- [8] B. Li, J. Deng, W. Zhang, Z. Liang, D. Du, X. Jin, and W. Zeng, "Hierarchical temporal context learning for camera-based semantic scene completion," *arXiv preprint arXiv:2407.02077*, 2024.
- [9] Y. Huang, W. Zheng, Y. Zhang, J. Zhou, and J. Lu, "Tri-perspective view for vision-based 3d semantic occupancy prediction," in *Proceedings of the IEEE/CVF conference on computer vision and pattern recognition*, 2023, pp. 9223–9232.
- [10] A.-Q. Cao and R. De Charette, "Monoscene: Monocular 3d semantic scene completion," in *Proceedings of the IEEE/CVF Conference on Computer Vision and Pattern Recognition*, 2022, pp. 3991–4001.
- [11] J. Yao, C. Li, K. Sun, Y. Cai, H. Li, W. Ouyang, and H. Li, "Ndc-scene: Boost monocular 3d semantic scene completion in normalized device coordinates space," in *2023 IEEE/CVF International Conference on Computer Vision (ICCV)*. IEEE Computer Society, 2023, pp. 9421–9431.
- [12] H. Jiang, T. Cheng, N. Gao, H. Zhang, T. Lin, W. Liu, and X. Wang, "Symphonize 3d semantic scene completion with contextual instance queries," in *Proceedings of the IEEE/CVF Conference on Computer Vision and Pattern Recognition*, 2024, pp. 20258–20267.
- [13] Y. Li, Z. Yu, C. Choy, C. Xiao, J. M. Alvarez, S. Fidler, C. Feng, and A. Anandkumar, "Voxformer: Sparse voxel transformer for camera-based 3d semantic scene completion," in *Proceedings of the IEEE/CVF conference on computer vision and pattern recognition*, 2023, pp. 9087–9098.
- [14] Y. Wang and C. Tong, "H2gformer: Horizontal-to-global voxel transformer for 3d semantic scene completion," in *Proceedings of the AAAI Conference on Artificial Intelligence*, vol. 38, no. 6, 2024, pp. 5722–5730.
- [15] Y. Zheng, X. Li, P. Li, Y. Zheng, B. Jin, C. Zhong, X. Long, H. Zhao, and Q. Zhang, "Monoocc: Digging into monocular semantic occupancy prediction," in *2024 IEEE International Conference on Robotics and Automation (ICRA)*. IEEE, 2024, pp. 18398–18405.
- [16] J. Li, K. Han, P. Wang, Y. Liu, and X. Yuan, "Anisotropic convolutional networks for 3d semantic scene completion," in *Proceedings of the IEEE/CVF Conference on Computer Vision and Pattern Recognition*, 2020, pp. 3351–3359.
- [17] R. Cheng, C. Agia, Y. Ren, X. Li, and L. Bingbing, "S3cnet: A sparse semantic scene completion network for lidar point clouds," in *Conference on Robot Learning*. PMLR, 2021, pp. 2148–2161.
- [18] Z. Li, W. Wang, H. Li, E. Xie, C. Sima, T. Lu, Q. Yu, and J. Dai, "Bevformer: learning bird's-eye-view representation from lidar-camera via spatiotemporal transformers," *IEEE Transactions on Pattern Analysis and Machine Intelligence*, 2024.
- [19] Z. Ye, T. Jiang, C. Xu, Y. Li, and H. Zhao, "Cvt-occ: Cost volume temporal fusion for 3d occupancy prediction," in *European Conference on Computer Vision*. Springer, 2024, pp. 381–397.
- [20] S. Wang, J. Yu, W. Li, W. Liu, X. Liu, J. Chen, and J. Zhu, "Not all voxels are equal: Hardness-aware semantic scene completion with self-distillation," in *Proceedings of the IEEE/CVF Conference on Computer Vision and Pattern Recognition*, 2024, pp. 14792–14801.
- [21] Y. Wu, Q. Wen, and Q. Chen, "Optimizing video prediction via video frame interpolation," in *Proceedings of the IEEE/CVF Conference on Computer Vision and Pattern Recognition*, 2022, pp. 17814–17823.
- [22] X. Hu, Z. Huang, A. Huang, J. Xu, and S. Zhou, "A dynamic multi-scale voxel flow network for video prediction," in *Proceedings of the IEEE/CVF Conference on Computer Vision and Pattern Recognition*, 2023, pp. 6121–6131.
- [23] M. Choi, H. Kim, B. Han, N. Xu, and K. M. Lee, "Channel attention is all you need for video frame interpolation," in *Proceedings of the AAAI conference on artificial intelligence*, vol. 34, no. 07, 2020, pp. 10663–10671.
- [24] L. Lu, R. Wu, H. Lin, J. Lu, and J. Jia, "Video frame interpolation with transformer," in *Proceedings of the IEEE/CVF Conference on Computer Vision and Pattern Recognition*, 2022, pp. 3532–3542.
- [25] A. Villar-Corrales, A. Karapetyan, A. Boltres, and S. Behnke, "Mspred: Video prediction at multiple spatio-temporal scales with hierarchical recurrent networks," *arXiv preprint arXiv:2203.09303*, 2022.
- [26] J. Park, J. Kim, and C.-S. Kim, "Biformer: Learning bilateral motion estimation via bilateral transformer for 4k video frame interpolation," in *Proceedings of the IEEE/CVF Conference on Computer Vision and Pattern Recognition*, 2023, pp. 1568–1577.
- [27] J.-Y. Franceschi, E. Delasalles, M. Chen, S. Lamprier, and P. Gallinari, "Stochastic latent residual video prediction," in *International Conference on Machine Learning*. PMLR, 2020, pp. 3233–3246.
- [28] B. Wu, S. Nair, R. Martin-Martin, L. Fei-Fei, and C. Finn, "Greedy hierarchical variational autoencoders for large-scale video prediction," in *Proceedings of the IEEE/CVF Conference on Computer Vision and Pattern Recognition*, 2021, pp. 2318–2328.
- [29] J. Ho, A. Jain, and P. Abbeel, "Denoising diffusion probabilistic models," *Advances in neural information processing systems*, vol. 33, pp. 6840–6851, 2020.
- [30] R. Rombach, A. Blattmann, D. Lorenz, P. Esser, and B. Ommer, "High-resolution image synthesis with latent diffusion models," in *Proceedings of the IEEE/CVF conference on computer vision and pattern recognition*, 2022, pp. 10684–10695.
- [31] A. Blattmann, R. Rombach, H. Ling, T. Dockhorn, S. W. Kim, S. Fidler, and K. Kreis, "Align your latents: High-resolution video synthesis with latent diffusion models," in *Proceedings of the IEEE/CVF conference on computer vision and pattern recognition*, 2023, pp. 22563–22575.
- [32] Y. Wei, L. Zhao, W. Zheng, Z. Zhu, J. Zhou, and J. Lu, "Surroundocc: Multi-camera 3d occupancy prediction for autonomous driving," in *Proceedings of the IEEE/CVF International Conference on Computer Vision*, 2023, pp. 21729–21740.
- [33] Y. Zhang, Z. Zhu, and D. Du, "Occformer: Dual-path transformer for vision-based 3d semantic occupancy prediction," in *Proceedings of the IEEE/CVF International Conference on Computer Vision*, 2023, pp. 9433–9443.
- [34] H. Xiao, H. Xu, W. Kang, and Y. Li, "Instance-aware monocular 3d semantic scene completion," *IEEE Transactions on Intelligent Transportation Systems*, vol. 25, no. 7, pp. 6543–6554, 2024.
- [35] J. Yao and J. Zhang, "Depthssc: Depth-spatial alignment and dynamic voxel resolution for monocular 3d semantic scene completion," *arXiv preprint arXiv:2311.17084*, 2023.
- [36] S. Ioffe and C. Szegedy, "Batch normalization: Accelerating deep network training by reducing internal covariate shift," in *International conference on machine learning*. pmlr, 2015, pp. 448–456.
- [37] X. Huang and S. Belongie, "Arbitrary style transfer in real-time with adaptive instance normalization," in *Proceedings of the IEEE international conference on computer vision*, 2017, pp. 1501–1510.
- [38] S. Wang, R. Clark, H. Wen, and N. Trigoni, "Deepvo: Towards end-to-end visual odometry with deep recurrent convolutional neural networks," in *2017 IEEE international conference on robotics and automation (ICRA)*. IEEE, 2017, pp. 2043–2050.
- [39] I. Loshchilov and F. Hutter, "Decoupled weight decay regularization," *arXiv preprint arXiv:1711.05101*, 2017.
- [40] K. He, X. Zhang, S. Ren, and J. Sun, "Deep residual learning for image recognition," in *Proceedings of the IEEE conference on computer vision and pattern recognition*, 2016, pp. 770–778.
- [41] F. Li, H. Zhang, H. Xu, S. Liu, L. Zhang, L. M. Ni, and H.-Y. Shum, "Mask dino: Towards a unified transformer-based framework for object detection and segmentation," in *Proceedings of the IEEE/CVF conference on computer vision and pattern recognition*, 2023, pp. 3041–3050.